BIOCHEMISTRY
including biophysical chemistry & molecular biology

ARTICLE

pubs.acs.org/biochemistry

Elucidation of the Protonation States of the Catalytic Residues in *mt*KasA: Implications for Inhibitor Design

Wook Lee,[†] Sylvia R. Luckner,[‡] Caroline Kisker,[‡] Peter J. Tonge,[§] and Bernd Engels*[,†]

[†]Institut für Physikalische und Theoretische Chemie, Universität Würzburg, Am Hubland, D-97070 Würzburg, Germany

[‡]Rudolf Virchow Center for Experimental Biomedicine, Institute for Structural Biology, University of Würzburg, Würzburg, Germany

[§]Institute for Chemical Biology and Drug Discovery, Department of Chemistry, Stony Brook University, Stony Brook, New York 11794-3400, United States

ABSTRACT: KasA (β-ketoacyl ACP synthase I) is involved in the biosynthetic pathway of mycolic acids, an essential component of the cell wall in *Mycobacterium tuberculosis*. It was shown that KasA is essential for the survival of the pathogen and thus could serve as a new drug target for the treatment of tuberculosis. The active site of KasA was previously characterized by X-ray crystallography. However, questions regarding the protonation state of specific amino acids, the orientation of the histidine groups within the active site, and additional conformers being accessible at ambient temperatures remain open and have to be addressed prior to the design of new inhibitors. We investigate the active site of KasA in this work by means of structural motifs and relative energies. Molecular dynamics (MD) simulations, free energy perturbation computations, and calculations employing the hybrid quantum mechanics/molecular mechanics (QM/MM) method made it possible to determine the protonation status and reveal important details about the catalytic mechanism of KasA. Additionally, we can rationalize the molecular basis for the acyl-transfer activity in the H311A mutant. Our data strongly suggest that inhibitors should be able to inhibit different protonation states because the enzyme can switch easily between a zwitterionic and neutral state.

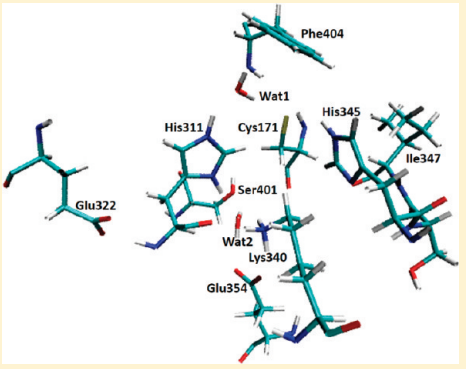

Mycobacterium tuberculosis is the causative pathogen of the disease tuberculosis (TB). According to a report by the World Health Organization, it was estimated that there were 9.2 million cases of new infections and 1.2 million fatal cases in 2006.[1] The emergence of multidrug-resistant strains of TB (MDR-TB) that are resistant to first-line antitubercular drugs, namely, rifampin and isoniazid, has made TB a more intractable disease.[2] To make matters worse, extensively drug-resistant tuberculosis (XDR-TB) strains discovered in 2005 are resistant not only to first-line antitubercular drugs but also to second-line antitubercular drugs such as fluoroquinolone, amikacin, kanamycin, and capreomycin.[3] The appearance of XDR-TB has emerged as a severe threat to human health and has underlined the importance of identifying new drug targets that are effective against all *M. tuberculosis* strains.

The mycobacterial cell wall is an essential component for survival of the pathogen, and mycolic acids are the most characteristic component of the mycobacterial cell wall. They are composed of extraordinarily long fatty acid molecules with 40−60 carbon atoms and a short branch of typically 24 carbons.[4] Mycolic acids have several important characteristics such as resistance to chemical injuries,[5] resistance to hydration,[6] and, most importantly, their low permeability that contributes to the intrinsic drug resistance of the pathogen.[7] Consequently, the enzymes involved in the biosynthetic pathway of mycolic acids gained attention as excellent targets for the development of new antimycobacterial drugs. A noticeable example of this is the first-line antitubercular drug isoniazid, which disrupts the integrity of the cell wall by inhibition of the enoyl-ACP reductase InhA, an enzyme that plays a significant role in the biosynthetic pathway of mycolic acids.[8]

The biosynthetic pathway of mycolic acids in *M. tuberculosis* requires two fatty acid synthesis (FAS) systems, namely, FAS-I and FAS-II.[9,10] The mammalian-like FAS-I system is encoded by a single gene producing a polypeptide that contains all of the necessary enzymatic activities and carrier functions.[11] On the other hand, the bacterial-type FAS-II system is encoded by several distinct genes that yield separate enzymes, each catalyzing a single step in the pathway.[12] The enzyme in each step interacts with the acyl carrier protein (AcpM) to transfer the growing fatty acyl chain from one enzyme to another.[13] The FAS-I system conducts de novo synthesis of fatty acids of intermediate length from acetyl-CoA,[11] and these products are further elongated in the FAS-II system until they reach a length of up to 56 carbons.[14] Subsequently, they are used as a building block for mycolic acids.

KasA is one of the main enzymes involved in the biosynthetic pathway of the FAS-II system. The depletion of KasA gives rise to cell lysis and eventually leads to cell death.[15] Thus, this enzyme has been considered as an attractive drug target for the treatment of tuberculosis. KasA catalyzes a condensation reaction in which it accepts the AcpM-bound acyl chain from InhA and elongates the acyl chain by two carbon atoms.[16] The reaction consists of three steps. In the first step, the acyl chain is covalently

Received: January 4, 2011
Revised: May 10, 2011
Published: May 26, 2011

ACS Publications © 2011 American Chemical Society

transferred from acyl-AcpM to the catalytic cysteine of the active site and AcpM is released. During the second step, a malonyl-AcpM binds to the active site and the malonyl group is decarboxylated to generate a carbanion with a concomitant release of carbon dioxide. In the last step, the carbanion attacks the acyl enzyme intermediate and the β-ketoacyl-AcpM and two additional carbon units can be released.[16]

The active site of KasA consists of a catalytic triad that is composed of one cysteine and two histidines. It is now widely accepted that the condensation reaction by KasA is initiated by the deprotonation of the catalytic cysteine.[17] Because of its relative position with respect to the catalytic cysteine, it was suggested that one of the catalytic histidines plays a role in abstracting a proton from the cysteine.[18,19] However, a mutagenesis study with KasI from *Escherichia coli* in which each catalytic histidine was mutated to an alanine showed that both histidine-substituted mutants still displayed acyl-transfer activity.[20] These results suggest that the helix macrodipole generated by the α-helix harboring the catalytic cysteine at its N-terminus is the primary reason for the stabilization of the cysteine thiolate in KasA. However, in contrast, a theoretical approach demonstrated that the stabilization of the zwitterionic form of the catalytic Cys-His dyad in cathepsin B is mostly due to the complex hydrogen bonding network while the helix macrodipole contributes only partially.[21]

In this study, we therefore addressed how the deprotonation of the catalytic cysteine is initiated in KasA from *M. tuberculosis*. First, we determined the correct protonation state of the catalytic residues in their resting state. Because His345, one of the catalytic residues, is in a different conformation compared to the same residue in other available KasA X-ray structures, we first checked whether the conformation of His345 in the X-ray structure of wild-type KasA is correct. Molecular dynamics (MD) simulations revealed that this residue has to assume a conformation in which it is rotated so that favorable interactions can be formed with the backbone. Additional MD simulations were performed for possible protonation states of the catalytic residues, and the results were compared to the X-ray structure. Free energy perturbation (FEP) simulations were performed to substantiate the findings made on the geometrical data. Simultaneously, a hybrid approach that combines quantum mechanical (QM) and molecular mechanical (MM) computations (QM/MM) was used to characterize the transfer of the proton from Cys171 to His311 and vice versa. In combination, we can show that KasA is most likely to be in a zwitterionic state in its resting state. Additionally, we investigated the molecular basis for acyl-transfer activity in the H311A variant.

MATERIALS AND METHODS

The initial structure for molecular dynamics (MD) simulations was obtained from the crystal structure of wild-type *M. tuberculosis* KasA [Protein Data Bank (PDB) entry 2WGD]. All MD simulations were performed using the NAMD 2.6 simulation package[22] in combination with the CHARMM 22 force field[23] with the CMAP correction.[24] The force field parameters for the thiolate ion in anionic cysteines were obtained from Foloppe et al.[25] TIP3P water molecules[26] were used for explicit solvent conditions. Each initial structure was solvated in a water shell with a radius of 45 Å. The water molecules were forced to stay inside the sphere during the simulation using spherical boundary conditions. After solvation, all systems were neutralized by adding an appropriate number of ions according to the total charge of the system using Autoionize version 1.1. Then, energy minimization was performed for 500 steps using the conjugate gradient method[27] to avoid any huge steric hindrance. A time step of 2 fs was used, and all chemical bonds containing hydrogen atoms were constrained using the RATTLE algorithm.[28] Nonbonded interactions were truncated at a cutoff distance of 12 Å, and the switching function was used to smoothly reduce the potential to zero at the cutoff distance. The temperature was gradually increased after minimization from 50 to 310 K while the protein was constrained in its initial position with a force constant of 24 kcal mol^{-1} $Å^{-2}$. Afterward, the force that was applied to the protein gradually decreased in a stepwise manner until it finally reached zero. Langevin dynamics was used to maintain the temperature constant. For a productive MD run, the first 1 ns was discarded for equilibration, and the following 5 ns were used for data gathering.

The FEP method[29] was employed to measure the relative free energy difference between different protonated systems. Because all FEP calculations were performed in an NVT ensemble, the obtained free energies are given as Helmholtz free energies. The devised thermodynamic cycle involves two alchemical transformations. The first calculation is for the reference system in which an individual residue with a neutral blocking group at both termini solvated in the water shell with a radius of 22 Å is gradually transformed from the protonated state to the deprotonated state. The second calculation simulates the same transformation but in the protein environment. A total of 118 windows of uneven width were introduced by adopting a set of intermediate mapping potentials between the start and the end point. For each window, 10 ps of equilibration and 30 ps of data collection were used, resulting in a total running time of 4.72 ns. Within a range of 0.1 from both end points of λ, a total of 84 windows were introduced to avoid an end-point catastrophe.[30] To estimate the accuracy of the calculation, each FEP calculation was repeated four times in one direction,[31] and 20 Å as a cutoff value was used for all FEP calculations to minimize any possible artifact from a short cutoff value.

During the process of transfer of a proton from one residue to the other, the cleavage and formation of covalent bonds are inevitable. For calculating the energy profile of this process occurring in the enzyme, the QM/MM optimization is a suitable choice because it not only can deal with the breakage and formation of a bond by quantum mechanics but also can take the enzyme environment into account by classical mechanics. The initial structures for QM/MM optimizations were taken from the MD simulation trajectory and subsequently minimized for 2500 steps using the conjugate gradient method.[27] In the QM/MM calculation, the entire enzyme and water molecules only within 25 Å of the active site were included. All QM/MM optimizations were conducted using Chemshell.[32] Cys171, His311, and a water molecule were involved in the QM region. The Turbomole program package[33] was used at the level of density functional theory for QM calculations. MM calculations were conducted with the DL_POLY code[34] in combination with the CHARMM force field. At the boundary of the QM and MM part, the charge-shift scheme was applied to prevent overpolarization.[35,36] A hybrid delocalized internal coordinate (HDLC) optimizer[37] was used for geometry optimization, and only water molecules and residues within 10 Å of the active site were involved in the optimization process while the remaining part was held fixed. Geometry optimizations in the QM part were performed with RI-DFT/B-LYP in combination with TZVP basis sets. For single-point calculations, the DFT/B3-LYP level was used with the same basis sets.

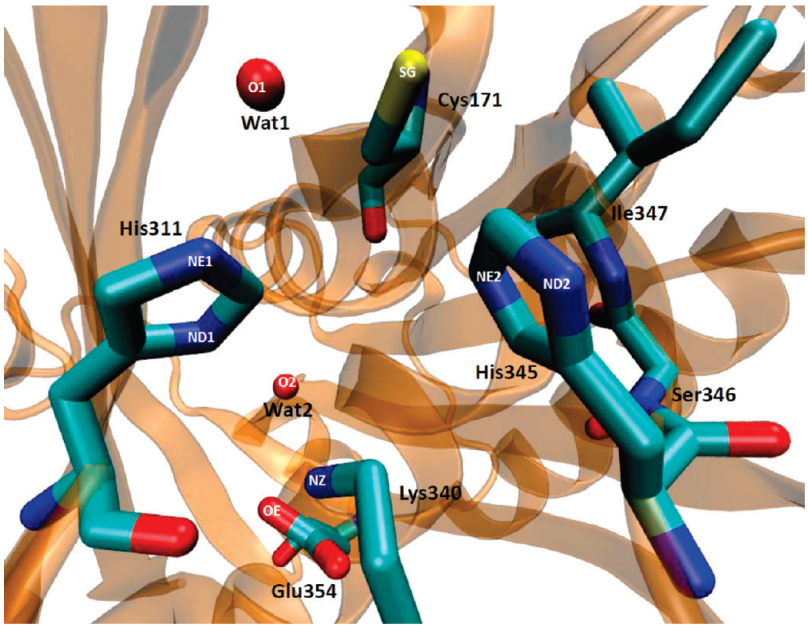

Figure 1. Active site of wild-type KasA.[42] The active site residues and water molecules are shown as sticks, and the protein surroundings are represented as a cartoon model. Labels for residue numbers and atoms are colored black and white, respectively.

Because of the strong dependence of QM/MM optimization on starting structures, sampling of the system was required. For this reason, we performed umbrella sampling in the context of the QM/MM scheme to compute the potential of mean force (PMF) surfaces for the proton transfer. They were performed using the Recife Model 1 (RM1) method[38] for QM, and the AMBER force field (FF99SB)[39] for the MM part. A total of 448 windows were employed for umbrella sampling, and the weighted histogram analysis method (WHAM) was applied to generate a PMF surface.[40] Then, 20 ps of equilibration and 30 ps of productive run were used for each window, and the force constants used were in the range of 800−900 kcal mol^{-1} $Å^{-2}$. To test the reliability of this semiempirical approach, we performed additional model computations involving the QM part of our QM/MM computations and neglecting environmental effects. These computations were performed with the Sander module of the AMBER 11 program package,[41,42] and the Turbomole program package.[33]

To test the importance of residues in terms of the difference in energy between the zwitterionic state and the neutral state, we used charge deletion analysis.[43−45] For this calculation, the partial charges of the corresponding residues in the MM part were set to zero and additional single-point QM/MM calculations were performed.

RESULTS

The active site of KasA consists of the three catalytic residues, Cys171, His311, and His345 (Figure 1). In addition to these residues, in most KasA crystal structures two additional water molecules complete the active site of KasA. They are assumed to play a significant role in catalysis, but details regarding their functions are not known. One water molecule (Wat1) is located between Cys171 and His311 in the proximity of both residues. The other water molecule (Wat2) is located 2.8 Å from the δ-nitrogen of His311. It also interacts with Lys340 and Glu354, which are conserved in all Kas enzymes. The roles of these two residues are also not exactly understood, but it has been reported that Lys340 significantly contributes to the maintenance of the structure of the active site.[46]

Orientation of the Imidazole Ring of His345. With respect to the orientation of the imidazole ring of His345, Luckner et al.[47] interpreted their data in wild-type KasA (PDB entry 2WGD) as shown in Figure 1. This conformation is flipped by 180° in comparison to other X-ray structures of the KasA enzyme from *M. tuberculosis* (PDB entries 2WGE, 2WGF, and 2WGG) or other KAS enzymes (PDB entries 1DD8, 1KAS, 1J3N, 1E5M, and 1OX0). It seems to be unfavorable because it does not allow the formation of a hydrogen bond between the δ-nitrogen of His345 and the backbone amide, which was postulated on the basis of other crystal structures. However, it would allow a hydrogen bond to the Cys171 residue, which is not possible in the other conformation. Because a reliable designation of the conformation on the basis of X-ray data alone is not possible, an incorrectly assigned conformation might have resulted. Hence, we performed MD simulations for each conformation in which either the δ- or ε-nitrogen of His345 was protonated. The resulting tautomers are shown in Figure 2. Because the protonation states of Cys171 and His311 may also affect the orientation of His345, their protonation states have to be taken into account, as well. According to usual pK_a values, one would assume that the sulfur center of Cys171 and the δ-nitrogen of His311 are protonated while the ε-nitrogen of His311 is expected to be deprotonated. Because the His311-Cys171 dyad is neutral in this case, this situation will be called the neutral state. However, in the resting states of various enzymes with Cys-His pairs, the proton is moved from the sulfur of the Cys to the ε-nitrogen of the His residue ($His311H^+/Cys171^-$). This situation will be called the zwitterionic state. It has been proposed in many mechanistic studies because the neutral state is not sufficiently reactive for the enzymatic reactions. To take mutual interactions into account, we performed MD simulations for all resulting protonation states.

If the δ-nitrogen is protonated (Figure 2, tautomer 1), the imidazole ring remained in the unusual conformation given by

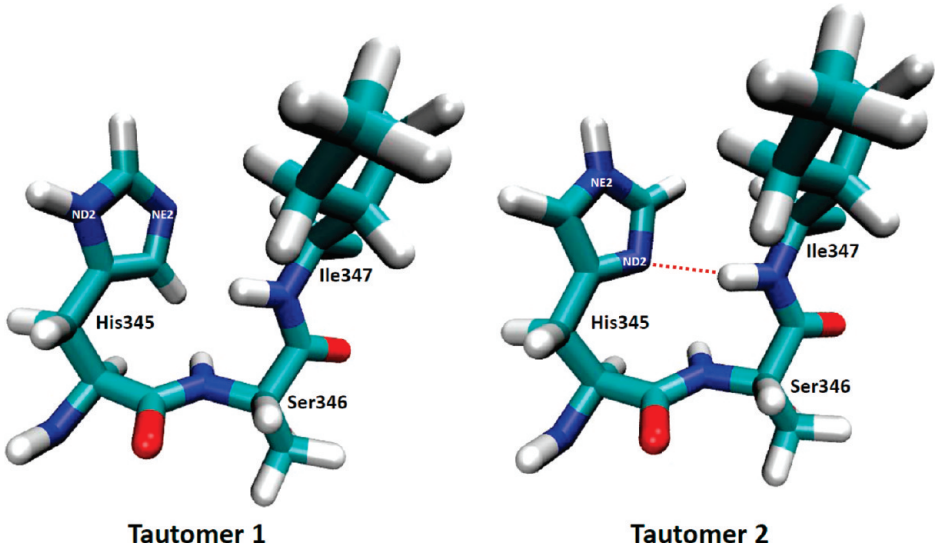

Figure 2. Possible tautomeric forms of His345. Tautomer 1 is derived from the unusual conformation of His345 in the crystal structure of wild-type KasA. Tautomer 2 describes the situation found in other crystal structures of KasA. In addition to His345, Ser346 and Ile347 are also shown to indicate possible interactions between His345 and the backbone of Ile347. The interaction is represented as a red dotted line.

Luckner et al.[47] for the entire simulation. For tautomer 2 in which the ε-nitrogen of His345 is protonated, the imidazole ring flipped during the simulation and turned into the conformation indicated in Figure 2. This conformation corresponds to the orientation described in previous crystal structures. This rotation is due to repulsive interactions between the hydrogen at the ε-nitrogen of His345 and the hydrogen of the backbone amide group. It is important to note that the different behaviors of the two tautomers were always observed regardless of whether the other two catalytic residues, His311 and Cys171, were in the neutral or zwitterionic state.

To determine which of the two tautomers is more likely, we monitored the movements of all neighboring residues during the MD simulation and compared them with the experimentally measured orientations. All of them adjust to the rotated conformation, but the position of the backbone of Ile347 is the decisive property with respect to the relative orientation of the imidazole ring of His345. This backbone rotation can be measured as changes in the φ and ψ dihedral angles of Ile347. The distributions of these dihedral angles during the MD simulations are plotted in Figure 3A for the neutral state of the His311-Cys171 dyad and in Figure 3B for the corresponding zwitterionic state. The crystal structure of Luckner et al.[47] shows that the backbone of Ile347 adopts an unusually strained conformation (φ = 25°, and ψ = −107°) as shown in the Ramachandran plot (Figure 3C). This unusual conformation is only found for tautomer 2 for which the maxima of the computed distributions are approximately 50° (φ) and −100° (ψ) if His311 and Cys171 adopt the neutral state and approximately 40° (φ) and −100° (ψ) if His311 and Cys171 are in the zwitterionic state. Figure 2 reveals that the hydrogen bond between His345 and the backbone amide of Ile347 acts as one of the constraints to maintain this strained conformation. Because of the protonation of the δ-nitrogen, this bond cannot be formed in tautomer 1. Thus, the strained backbone turns into the conformation that belongs to the regular α-helical region in the Ramachandran plot. The resulting maxima of the computed distribution for tautomer 1 are approximately −60° (φ) and −50° (ψ) for the neutral state and approximately −70° (φ) and −50° (ψ) for the zwitterionic state. They deviate from the measured values by approximately −80° (φ) and 50° (ψ), respectively. On the basis of the agreement with the unusual conformation of Ile347, we conclude that tautomer 2 represents the situation from the crystal structure given by Luckner et al.[47] This means that the imidazole ring is flipped by 180° in comparison to its original position. However, both conformations would have explained equally well the electron density maps and could not have been discerned in the crystal structure.

MD Simulations for Identifying the Preferred Protonation State of His311. So far, we could substantiate the orientation and protonation of His345, but because of the weak influence on the protonation state of the catalytic His311-Cys171 dyad, their state remains to be determined. For the investigation of the protonation status of His311, we took three different tautomers into account. In the zwitterionic state of the His311-Cys171 dyad described above, both nitrogen centers of the imidazole ring of His311 are protonated (Figure 4A). In the corresponding neutral state, only the δ-nitrogen center is protonated. Additionally, we considered the situation in which only the ε-nitrogen center is protonated (Figure 4B). We used the same strategy that was employed for His345 and monitored the movements of all neighboring residues and compared the data with their experimental counterparts. The distance between the oxygen center of the second water molecule (Wat2) and the ε-nitrogen of His311 allowed a first determination of the protonation state of His311. According to the crystal structure, the distance is ∼2.8 Å, which indicates a hydrogen bond. During the MD simulations of the ionic and neutral state in which the δ-nitrogen of His311 is protonated, the distances between these two atoms fluctuated around this value (Figure 4C). Note that the distance distribution found for the zwitterionic state agrees better with the X-ray data than those of the neutral counterpart. However, the difference between both is too small for a definitive answer. If only the ε-nitrogen center is protonated (Figure 4B), the maximum of the distance distribution increases to ∼3.3 Å and becomes considerably broader. The increase in the distance and the broadening take place because the hydrogen bond between both centers is no

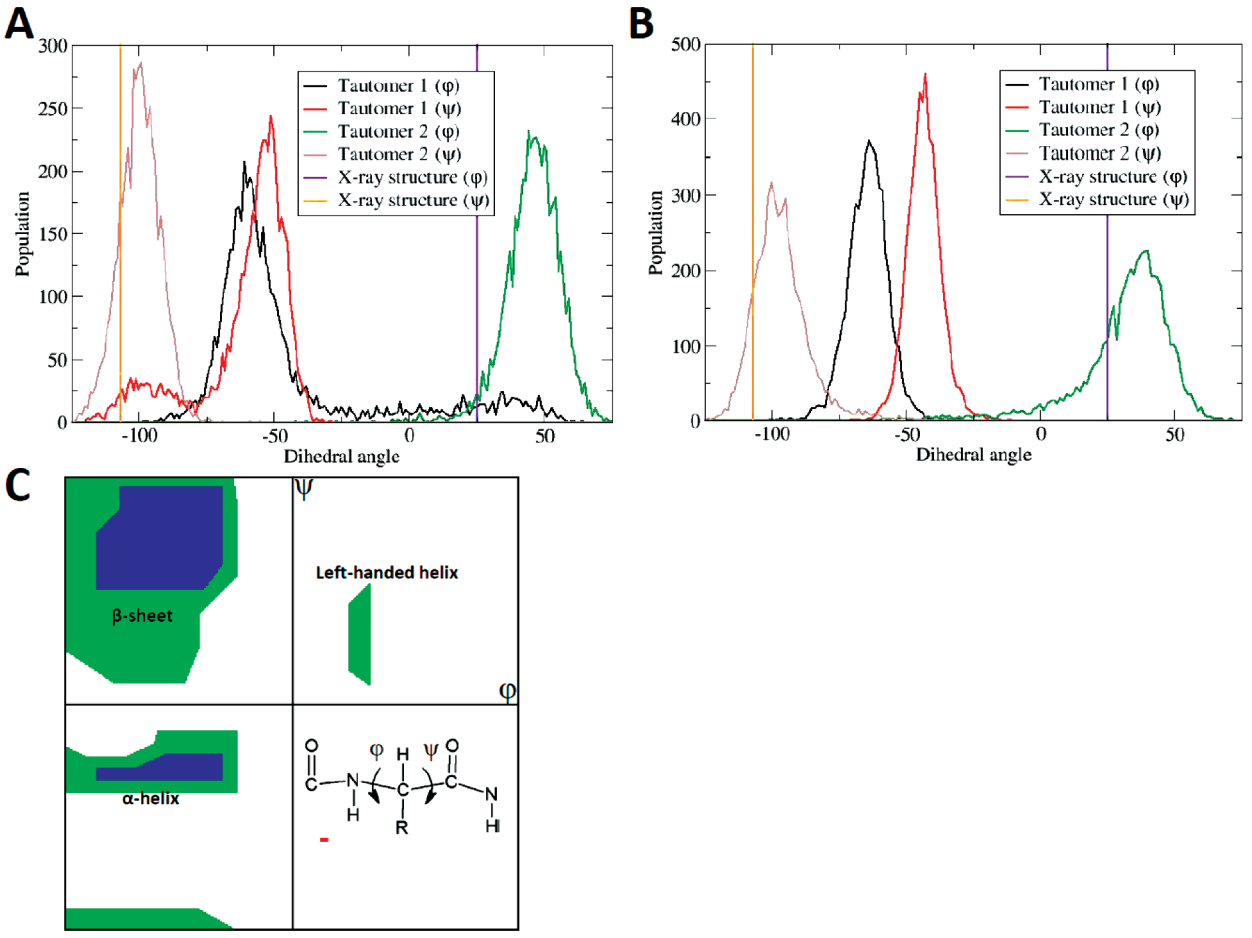

Figure 3. Backbone φ and ψ angle distributions of Ile347 during the MD simulations of the two tautomeric forms of His345 given in Figure 2. The measurements were performed for the neutral (A) and zwitterionic (B) state. The φ and ψ angles from the crystal structure are also shown as vertical lines for comparison. The Ramachandran plot of Ile347 from the crystal structure is represented as a red dot in C, and the positions of the φ and ψ angles in the protein backbone are shown in the inset.

longer possible (Figure 4B). The strong deviations between measured and computed data indicate that a protonated ε-nitrogen of His311 can be ruled out. The protonation of His311 corresponds either to the ionic state (both nitrogen centers protonated) or to the neutral state (only the δ-nitrogen protonated). This is also in line with the observation that the δ-nitrogen of the corresponding histidine residue in *Sp*FabF showed substantial electron density in the 1.3 Å crystal structure.[48]

The investigation also sheds some light on the role of the Wat2 molecule conserved in most Kas enzymes and the functions of Glu354, Lys340, and Ser401. Wat2 represents an important anchor for His311. It seems to fix His311 in a position that is necessary for the function of the enzyme. To execute this function, Wat2 must also be fixed. Wat2 is located in the center of a hydrogen bonding network that comprises Glu354, Lys340, and Ser401. The two former residues form strong hydrogen bonds to Wat2 through the ammonium group of Lys340 and the carboxylate moiety of Glu354. The salt bridge between these two groups further strengthens this network and rigidifies it. The final interaction of Wat2 results from the hydrogen bond to Ser401. To test this observation, we performed an MD simulation without Wat2. During this simulation, the imidazole ring of His311 and various other residues changed their orientation so strongly that the enzyme became inactive. This indicates that Wat2 represents an important factor for the stabilization of the active site. The hydrogen bond between the ammonium moiety of Lys340 and the oxygen center of the backbone carbonyl group of His311 represents a second anchor for the imidazole ring of His311. However, Wat2 seems to be more important because it is in direct contact with the imidazole ring. In contrast, the backbone carbonyl group of His311 is separated from the imidazole ring by two CH_2 groups. Hence, this interaction can induce less rigidity.

MD Simulations for Identifying the Preferred Protonation State of the Cys171-His311 Dyad. So far, we have clarified the protonation status of His345 and substantiated that the δ-nitrogen of His311 is also protonated. As discussed above, the protonation state of the remaining ε-nitrogen of His311 is closely related to the protonation state of Cys171. The structural arrangement in the crystal structure (Figure 1 and Table 1) indicates that both residues interact with each other through a water molecule (Wat1). Because the δ-nitrogen of His311 was shown to be protonated, the question about the protonation status of His311 and Cys171 is narrowed down to the situations depicted in Scheme 1. The positively charged state (Scheme 1, left-hand side) is expected for environments with lower pH values. The negatively charged state (Scheme 1, right-hand side) will appear at high pH values. Neutral and zwitterionic states will be found between those environments, but the actual

dx.doi.org/10.1021/bi200006t |*Biochemistry* 2011, 50, 5743–5756

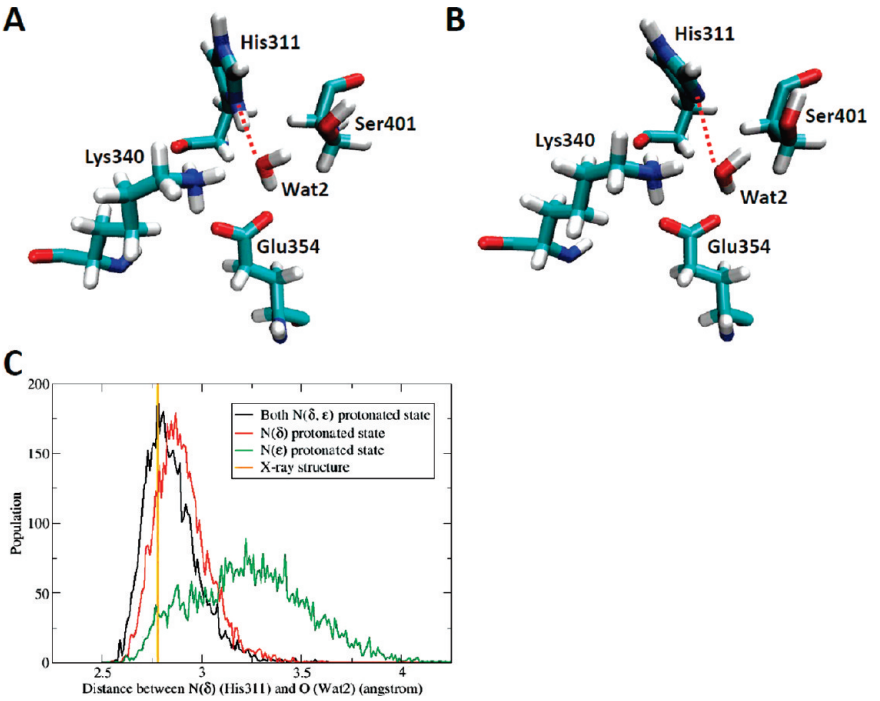

Figure 4. Interaction of His311 with a water molecule (Wat2) according to the change in the protonation state of His311. Structure A sketches the geometrical arrangement when the δ- and ε-nitrogen atoms of His311 are protonated, and sketch B indicates the structure if only the ε-nitrogen is protonated. Each picture was created from a representative frame of MD simulation results. The distances between the δ-nitrogen of His311 and the oxygen of the water molecule (dotted red lines in panels A and B) recorded during the MD simulation for each protonation state are plotted as corresponding distributions in panel C. The distance from the crystal structure is also given as a vertical line for comparison.

Table 1. Selected Distances of Important Pairs Depicted in Figure 1[a]

pair	distance (Å)	pair	distance (Å)
SG−NE2	3.6	ND1−O2	2.8
SG−O1	3.2	O2−NZ	3.0
O1−NE1	2.8	O2−OE	3.0

[a] All distances were extracted from the crystal structure of wild-type KasA.

protonation state of the resting state is unknown. Its determination is possible through the crystallographic data because they were obtained at pH 7.5. Considering the standard pK_a values of the involved residues (6.04 and 8.14 for the imidazole ring of His311 and the thiol moiety of cysteine, respectively) at this pH value, a neutral state is expected. For the active site of the KasA enzyme, however, the question remains open because the protein environment quite often affects the pK_a values considerably. To identify possible structural differences between the various protonation states, we used the same strategy as before and compared structural changes observed during the MD simulations with the corresponding experimental data. In this case, the orientation of the neighboring His345 (Figure 5) allows the determination of the protonation state of the His311-Cys171 dyad. If the sulfur center of Cys171 is protonated (thiol functionality), which is the case for the neutral and positively charged states, the N_ε-H group of His345 is oriented toward the oxygen center of Wat1 (Figure 5A) and forms a hydrogen bond with the water molecule. If Cys171 is deprotonated (thiolate functionality), which is found for the zwitterionic and negatively charged states, the N_ε-H group of His345 is directed toward the negatively charged sulfur center. The resulting hydrogen bond is considerably stronger because of the negative charge on the sulfur (Figure 5B). A visual inspection of the crystal structure (Figure 1) indicates that His345 is pointing toward Cys171. Hence, we expect that the crystal structure indicates that the KasA enzyme is in the zwitterionic or negatively charged state.

A quantification of the orientation of His345 is best obtained through the distance between the ε-nitrogen of His345 and the sulfur of Cys171. Other structural parameters, e.g., dihedral angles involving parts of the imidazole ring and the neighboring CH_2 group, provided less definite answers. The corresponding distance distributions for the four different states are given in Figure 5C. The peak of the distribution found for the zwitterionic state agrees perfectly with the corresponding measured distance of 3.36 Å. Also for the negatively charged state, Cys171 possesses a thiolate group. It is therefore not surprising that the distance distribution resembles that found for the zwitterionic state. Note that not only the distance but also the whole orientation of His345 is quite similar in both protonation states. However, the maximum of the distance distribution is longer (≈3.5 Å). The maximum of the distance distribution computed for the neutral state is ∼3.6−3.7 Å. It differs significantly by ∼0.3−0.4 Å from the experimentally measured distance. Because of these differences and on the basis of the overall orientation of His345 (Figure 4A,B), we rule out the neutral state. Note that the distance distribution function computed for the neutral state is broader than the distance distributions found for the zwitterionic and negatively charged states. The increased broadness results from the hydrogen bond between the N_ε-H group of His345 and the oxygen center of Wat1. This bond is considerably weaker than the bond formed in

dx.doi.org/10.1021/bi200006t |*Biochemistry* 2011, 50, 5743–5756

Scheme 1. Representation of the Four Different Protonation States

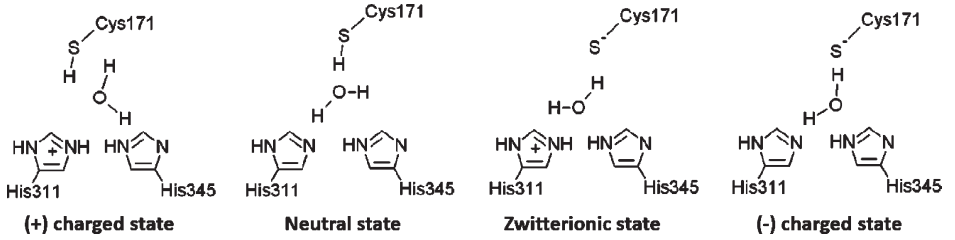

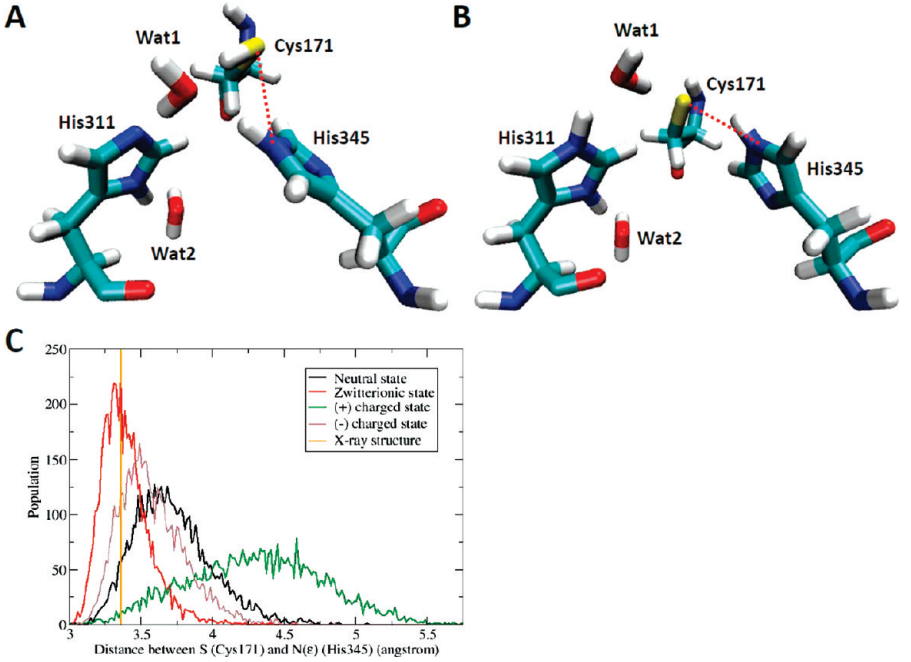

Figure 5. Change in the relative orientation of Cys171 and His345 according to the change in their protonation state. Panel A provides a representative structure of the active site in the neutral state, and panel B sketches the situation for the zwitterionic state. The distances between the sulfur of Cys171 and the ε-nitrogen of His345, which are shown as red dotted lines in panels A and B, are plotted as corresponding distributions in panel C.

the other two states. On the basis of the distance distributions, the positively charged state can be ruled out. Moreover, for this state, the water molecule that stayed between Cys171 and His311 at the beginning of the MD simulation moved away. This result would also be in conflict with the X-ray data where a water molecule builds a bridge between His345 and Cys171.

FEP Calculations for Evaluating the Perturbed pK_a Value of His311. The geometrical data indicate so far that the zwitterionic state is the most likely in the crystal structure. However, the data computed for the negatively charged state do not differ significantly from the experimental data. To substantiate that indeed the zwitterionic state is present, we performed FEP calculations to estimate the pK_a value of His311 in the protein environment. This in turn allows us to determine which of both states is most likely populated under a given experimental condition. The results from these calculations are listed in the first column of Table 2, while the thermodynamic cycles designed for these calculations are shown in the top part of Figure 6. In the top process, we alchemically protonated the N_ε center of His311 to N_ε-H to obtain a positively charged His311. In the standard approach, the influence of the enzyme environment on the pK_a value is estimated by the equation

Table 2. Free Energy Differences Obtained from the Free Energy Perturbation Method[a]

	top cycle	bottom cycle
ΔA^P	12.5 ± 1.0	−66.0 ± 0.5
ΔA^R	7.5 ± 1.6	−68.3 ± 0.9
$\Delta\Delta A$	5.0 ± 1.9	2.3 ± 1.0

[a] Each column represents calculated values for corresponding thermodynamic cycles shown in Figure 6. Four independent runs were performed for each calculation, and the standard deviations from these runs are also presented. All energies are given in kilocalories per mole.

$\Delta pK_a = (q \times \Delta\Delta G)/(2.303kT)$, where $\Delta\Delta G = \Delta G_1^P - \Delta G_1^R$ and q represents the charge of the ionized form of the relevant residue. ΔG_1^P and ΔG_1^R are the Gibbs free energies that correspond to the free Helmholtz energies depicted in Figure 6. Gibbs and Helmholtz free energies are connected by the term $p\Delta V$, with ΔV being the change in volume in the examined processes. The ΔV values of both described processes should be very similar. So, the use of $\Delta\Delta A$ instead of $\Delta\Delta G$ should not considerably enlarge the error bars of the computations.

dx.doi.org/10.1021/bi200006t |*Biochemistry* 2011, 50, 5743–5756

The FEP computations predict a $\Delta\Delta A$ value of 5.0 kcal/mol that corresponds to a pK_a shift of 3.5. Because of the resulting pK_a value of 9.5, His311 is expected to be completely protonated at pH 7.5. Even if $\Delta\Delta A$ has been overestimated by a factor of 2 for a pH of 7.5, His311 would still be mainly protonated. Hence, the FEP computations are in line with the geometrical data indicating that the zwitterioinic state was present in the X-ray experiment performed by Luckner et al.[47]

Our investigations indicate that the His311-Cys171 dyad adopts a zwitterionic situation. However, if the zwitterionic situation and the neutral situation differ only slightly in energy, the enzyme can switch between both quite easily by a proton transfer mediated by Wat1. Considering the strong changes in the geometrical orientation of His345, its movement could induce the switch. Hence, the difference in energy between the neutral and zwitterionic situations is important for mechanistic considerations. It is also of interest for the development of new drugs because the zwitterionic state and the neutral state represent considerably different environments for potential binders. If only one state is energetically accessible, the binders should be optimized for this state. If, however, the enzyme can easily switch between both states, the binders should be somehow adequate for both situations. The difference in energy between the neutral state and the zwitterionic state is indirectly accessible from FEP if the neutral state is also compared with the negatively charged state. We performed such calculations, but the lack of precision[31] made it impossible to resolve this issue.

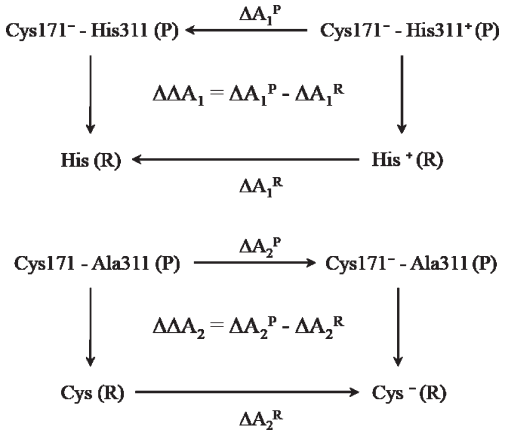

Figure 6. Thermodynamic cycles devised to obtain the perturbed pK_a value in the protein environment. The top cycle is for computing the shifted pK_a value of His311 to find the preferred state between the zwitterionic and negatively charged state, and the bottom cycle is for computing the shifted pK_a value of Cys171 in the H311A mutant. (R) represents the reference system, and (P) represents the protein environment.

Computations for Estimating the Difference in Energy between Neutral and Zwitterionic States. Because the corresponding FEP computations were not sufficiently reliable, we decided to substantiate the difference in energy between the neutral state and the zwitterionic state by means of independent methods. We used QM/MM optimization, which in previous studies was often able to provide reliable information about this topic. As a first step, we characterized the proton transfer by computing potential energy surfaces (PESs) using the distance between the ε-nitrogen of His311 and the hydrogen of Wat1 ($N_{His311}-H_{Wat1}$) and the distance between the oxygen of Wat1 and the hydrogen of Cys171 ($O_{Wat1}-H_{Cys171}$) as reaction coordinates. Both internal reaction coordinates were varied independently, while all other coordinates (in the following called secondary coordinates) are simply relaxed for both reaction coordinates. The results that are summarized in Figure 7 show that for the KasA enzyme the relative energetic positions of the zwitterionic state and the neutral state strongly depend on the preparation of the system. These preparations involve extensive MD simulation to adapt the whole system to the respective state. If the computations are initiated from the system prepared for the zwitterionic state, the zwitterionic state is lower in energy than the neutral state by ~9 kcal/mol. In contrast, if the computations are started from the system prepared for the neutral state, the neutral state is lower in energy by 5 kcal/mol. This indicates that the relative energy of both states strongly depends on the surroundings; therefore, these QM/MM optimizations are not able to determine the difference in energy between both states reliably. However, they allow some important conclusions about

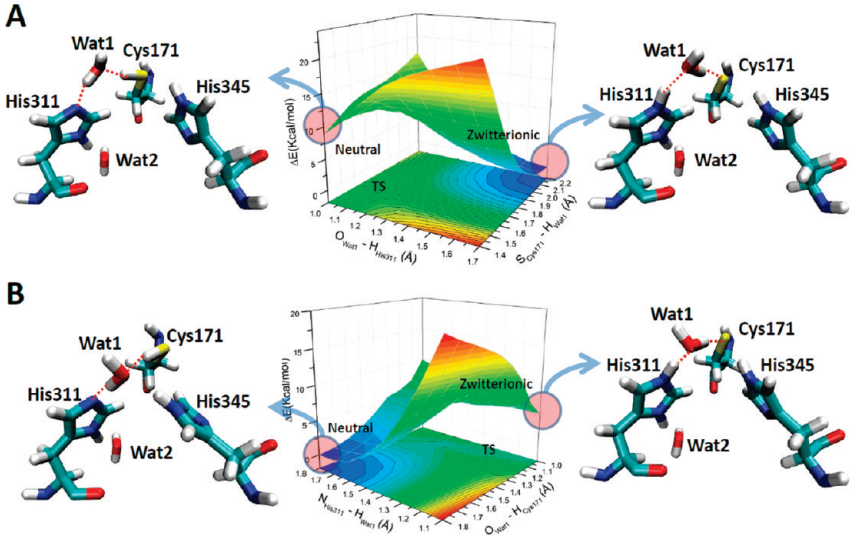

Figure 7. Potential energy surface (PES) for proton transfer from QM/MM calculations. The starting frames for generating PES in panels A and B were taken from the MD simulation of the zwitterionic state and the neutral state, respectively. The structural arrangement of the active site in both end states from each PES is also given, and the hydrogen bonds between QM residues are shown as red dotted lines.

dx.doi.org/10.1021/bi200006t |*Biochemistry* 2011, 50, 5743–5756

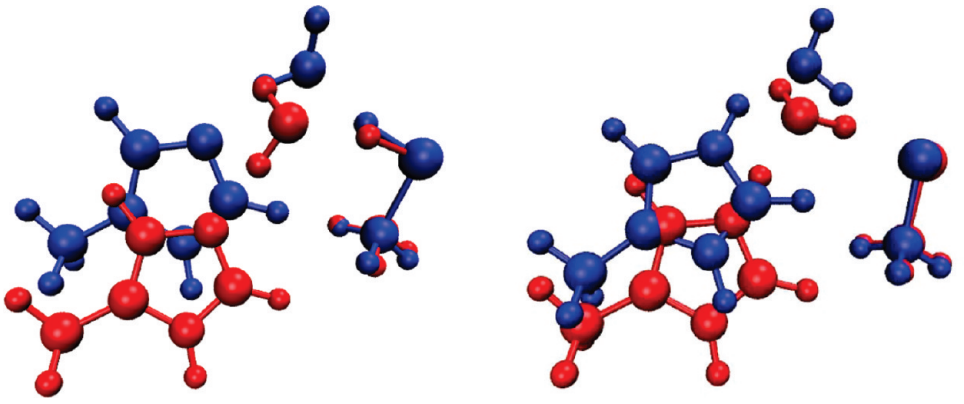

Figure 8. Geometrical orientations of the QM calculations for the neutral state (left) and zwitterionic state (right). Blue and red indicate the orientations that are obtained if the computations start from the zwitterionic state and the neutral state, respectively.

the KasA enzyme to be made. They clearly indicate that both states are quite close in energy, and in addition, the QM/MM optimization also suggests that the KasA enzyme is able to switch between both states by adapting the orientation of the various residues and water molecules to the respective situation.

An analysis of the geometry variations allows deeper insight into this capability to be gained. The variations in the geometries involve the QM part of the computation containing the bridging water molecule Wat1, His311, and Cys171 (Figure 8) and the surrounding residues that were taken into account using MM (Figure 7). Let us first concentrate on the variations found within the QM part (Figure 8). If the computations are started from the system prepared for the zwitterionic state, one hydrogen atom of the bridging water molecule points toward the thiolate group of Cys171 while the oxygen atom is directed toward the N_ε-H group (Figure 8, blue part on the right-hand side). If we now move along the surface given in Figure 7A toward the neutral state, the orientation of the Wat1 molecule adapts to the situation (Figure 8, blue part on the left-hand side). It is rotated slightly so that now one hydrogen atom points toward the N_ε center of His311 while the oxygen is directed toward the thiol group of Cys171. It is important to note that the relative orientations of His311, Cys171, and the center of mass of Wat1 do not change considerably.

If the system is prepared for the neutral state, we obtain a different geometrical orientation within the QM part (in Figure 8, compare the blue and red parts on the left-hand side). While the orientations of Wat1 with respect to the N_ε center of His311 and the thiol group of Cys171 closely resemble the blue and red sketched geometries, the relative orientation of His311 and Wat1 with respect to the Cys171 residue is different. Both are shifted downward. The fact that this orientation is not obtained in the computations starting from the zwitterionic state shows that both geometrical orientations are separated by a reaction barrier. If we now start from the red orientation (Figure 8, red part on the left-hand side) and move along the surface given in Figure 7B toward the zwitterionic state (Figure 8, red part on the right-hand side), the water reorients, but again the relative orientations of His311, Cys171, and the center of mass of Wat1 do not adapt to the situation found if the whole system was completely optimized for the zwitterionic state (Figure 8, blue part on the right-hand side). Again blue and red orientations are separated by a potential energy barrier. Please note that the orientation of the water molecule Wat1 also differs.

From the surrounding residues, His345 shows a quite distinct behavior. If the system is prepared for the zwitterionic state (Figure 7A, right-hand side), the N_ε-H group of His345 points toward the thiolate group of Cys171. If we move along the computed surface to the neutral state, the N_ε-H group of His345 is still oriented toward the sulfur center of Cys171. However, if the system is prepared for the neutral situation (Figure 7B, left-hand side), His345 is oriented differently. In this geometry, it points toward the oxygen center of Wat1. Again both geometrical orientations sketched in Figure 7 on the left-hand side (A vs B) are obviously separated by a barrier so that the lower one cannot be reached by a simple relaxation of all secondary parameters. If we now start from the system prepared for the neutral state and move toward the zwitterionic state (Figure 7B), His345 is reoriented, but perhaps because of its influence, Wat1 does not adopt the orientation that is found if the system is prepared for the zwitterionic state (Figure 7, panel A vs panel B on the right-hand side).

The analysis of the various geometries indicates that KasA can switch between the zwitterionic state and the neutral state quite easily because it needs only slight modifications to stabilize one state with respect to the other. The analysis indicates that the movements of His345 and Wat1 play a central role; however, the orientations of other residues also contribute and remain to be analyzed in detail.

The analysis also indicates that the potential energy surface describing the transfer of a proton from Cys171 to His311 is very rugged so that a projection of the multidimensional PES on the subspace spanned by the $N_{His311}-H_{Wat1}$ and $O_{Wat1}-H_{Cys171}$ distances is not sufficient to estimate the difference in energy between the neutral state and the zwitterionic state. To overcome this limitation, we used the umbrella sampling method in combination with a QM/MM scheme. This method can overcome the mentioned barriers because it not only relaxes all secondary parameters but also performs a MD sample for each point of the hypersurface. Furthermore, it can be used to compute the free energy. Because of the necessary sampling currently available, ab initio methods are too expensive for this type of calculation; therefore, semiempirical methods have to be employed for the QM part. To estimate the accuracy of available approaches, we compared the predictions of several semiempirical methods for the difference in energy between the neutral state and the zwitterionic state with the corresponding result of the B3LYP/TZVP approach. The computations were performed

Table 3. Comparison of the Results from Single-Point Calculations in the Gas Phase between Semiempirical and DFT Methods[a]

theory	ΔE_1	ΔE_2
AM1	32.3	64.7
PM3	37.4	50.6
PDDG-PM3	39.1	61.9
SCC-DFTB	not converged	–
RM1	25.0	41.5
B3LYP	22.9	61.2
B3LYP-D	22.8	60.8

[a] ΔE_1 represents the difference in energy between the neutral state and the zwitterionic state. ΔE_2 represents the difference in energy between the neutral state and the intermediate as indicated in Figure 10. All energies are given in kilocalories per mole.

for the QM part of our previous QM/MM optimizations neglecting further environmental effects (Table 3). The results indicate that the RM1 method seems to be well suited to estimate the difference in energy between the zwitterionic form and the neutral form. The comparison also underlines that RM1 strongly overestimates the stability of the intermediate state that involves hydronium ions. We started the umbrella sampling at the system prepared for the neutral state to exclude a bias toward the zwitterionic state.

The corresponding PMF surface for proton transfer is shown in Figure 9. The reaction coordinates in this computation were defined as the difference between two internal coordinates. For the first reaction coordinate, the difference between the $S_{Cys171}-H_{Cys171}$ and $H_{Cys171}-O_{Wat1}$ internal coordinates was used. The second reaction coordinate represents the difference between the $O_{Wat1}-H_{Wat1}$ and $H_{Wat1}-N_{His311}$ coordinates. The predicted stable intermediate represents an artifact of the RM1 method. As already mentioned, this method strongly overestimates the relative stability of this part of the surface (Table 3) but should be well suited to estimate the difference in energy between neutral and zwitterionic states. The computations predict that the zwitterionic state is ~0.4 kcal/mol lower in energy than the neutral state. However, the zwitterionic state should be slightly more stable. RM1 seems to underestimate the relative stability of the zwitterionic state with respect to the neutral one. In vacuum computations summarized in Table 3 (RM1), this underestimation amounts to ~2 kcal/mol in comparison to the value determined by the B3LYP/TZVP approach. If this error were transferred to the situation within the enzyme, the zwitterionic state would be 2–3 kcal/mol more stable than the neutral state. This may represent an upper bound for the energy difference because the error may be smaller in the enzyme because of error cancellations.

Nevertheless, such small energy differences are still within the uncertainties of the employed methods. Hence, it is important to note that the predictions obtained from the PMF surface agree nicely with those based on our simulations of the geometrical parameters. These simulations indicated that the zwitterionic state is observed in the X-ray data, and they point out that neutral and zwitterionic states differ in several geometrical parameters. Because of these differences, a population of both states should be seen in the X-ray data if the neutral state is populated by at least 10–20%. Using the Boltzmann distribution for the temperature at which the X-ray experiments were performed (100 K), such

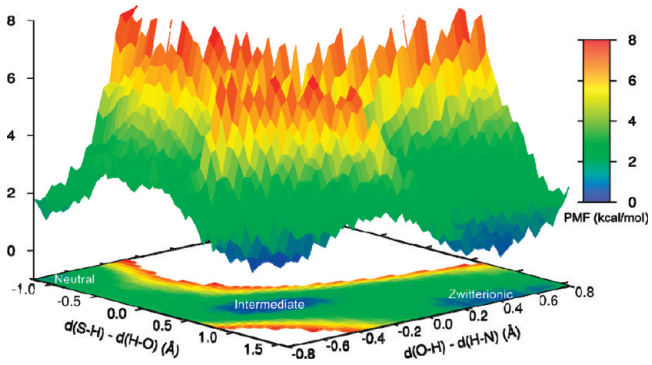

Figure 9. PMF surface for proton transfer generated from QM/MM computations in combination with the umbrella sampling method. Those parts of the surface that are more than 8 kcal/mol higher in energy than the zwitterionic state were omitted for a better description of the surface of interest.

Table 4. Contributions from Surrounding Residues in the MM Part of the QM/MM Computations for Stabilizing the Zwitterionic State Relative to the Neutral State[a]

residue switched off	ΔE (zwitterionic surroundings)	ΔE (neutral surroundings)
α-helix except Cys171	0.7	0.5
NH group of Cys171	2.6	3.5
Thr313	−1.0	−0.2
Glu322	7.6	6.9
Lys340	−5.7	−6.1
His345	6.2	4.9
Glu354	2.2	4.5
Ser401	0	0.4
Phe402	0.2	−1.9
Phe404	1.8	0.9
Wat2	1.5	3.5

[a] These energy contributions were calculated using the charge deletion method. All energies are given in kilocalories per mole. In both columns, the positive sign means that a given residue contributes to the stabilization of the zwitterionic state.

populations can be converted to a difference in energy of 0.4–0.3 kcal/mol between the zwitterionic and neutral states. Hence, because the X-ray experiments do not indicate that both states are populated, their energy difference must be at least 0.3–0.4 kcal/mol. These values represent the lower bound for the energy difference and again agree nicely with our computations. Please note that both states should be populated at a body temperature of 310 K. For the lower bound, the neutral state will be populated by ~35%. At an energy difference of 2 kcal/mol (upper bound), the neutral state would still be populated by ~5%.

Charge Deletion Analysis for Estimating the Contributions from Each Surrounding Residue to Stabilization of the Zwitterionic State. The stability of the zwitterionic state with respect to the neutral state is determined by additional residues. This is summarized in Table 4 with the results of a charge deletion analysis of the relative energies of both states. Note that this table cannot include the influence of His311 and Wat1 because they belong to the QM part of the QM/MM calculations. The moieties of Glu322, Lys340, and His345 seem to have

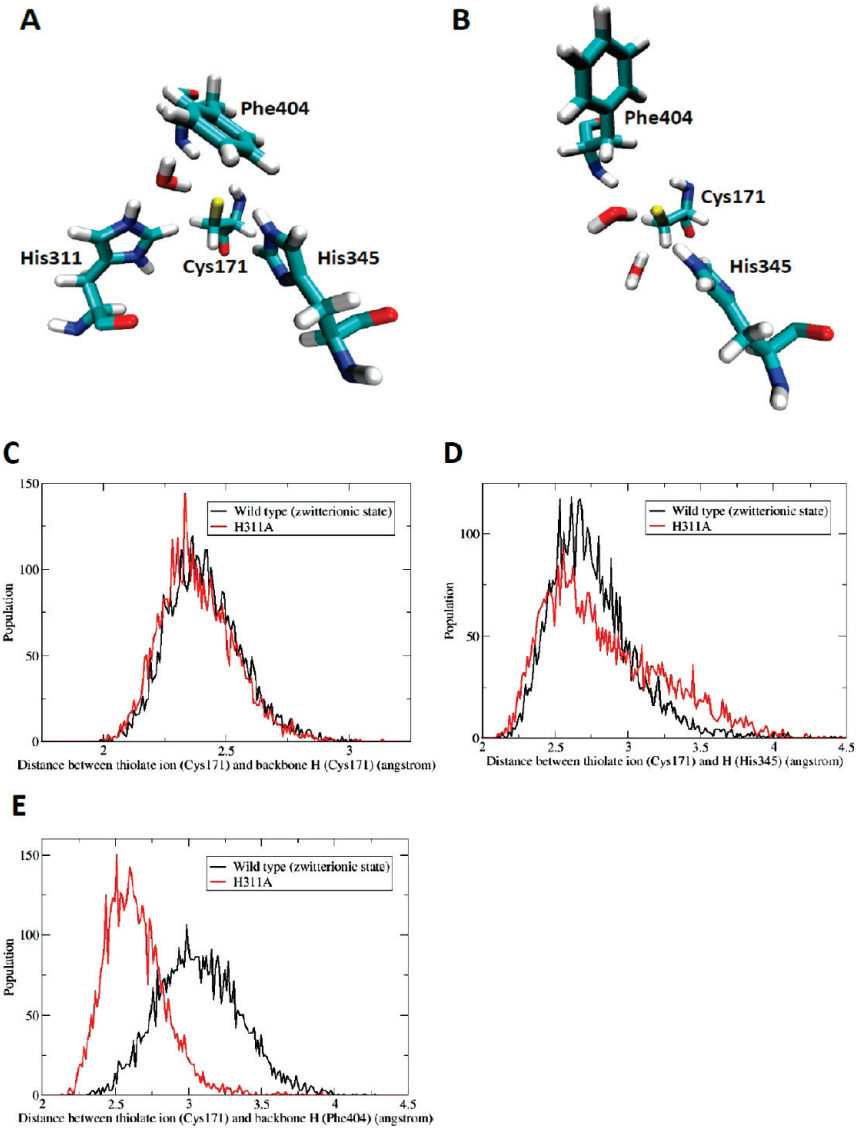

Figure 10. Difference in the hydrogen bonding network between wild-type KasA (zwitterionic state) and the H311A mutant. The geometrical arrangements of Cys171 and surrounding residues stabilizing the thiolate form of Cys171 in wild-type KasA and H311A are shown in panels A and B, respectively. The distance distributions for hydrogen bonds provided by the backbone amide of Cys171, His345, and the backbone amide of Phe404 are plotted in panels C−E, respectively.

the largest effects. The influence of Glu322 and His345 is obvious because they are in direct contact with either Cys171 or His311. His345 stabilizes the negatively charged Cys171 through a hydrogen bond. Glu322 seems to enhance the basicity of His311, thereby promoting the abstraction of the proton from Cys171 by His311. Lys340 destabilizes the zwitterionic state because it is positively charged itself. The size of this effect could result from a direct interaction of Lys340 with the carbonyl backbone group of His311 and indirectly via Wat2. One would expect a stronger influence of the oxyanion hole that consists of the NH backbone groups of Phe404 and Cys171. However, if these charges are switched off, the missing influence could be compensated by other residues in close contact with the thiolate group. This would be in line with the polarizability of the sulfur center. It is also possible that the stabilization effect of the oxyanion hole is similar for the zwitterionic state and the neutral state.

MD Simulations for Investigating the Unexpected Acyl-Transfer Activity in the H311A Variant. All MD simulation results so far support the idea that the zwitterionic state is most probably the resting state. Additionally, QM/MM computations showed that the zwitterionic state can be easily achieved by the transfer of a proton from Cys171 to His311. However, previous mutational experiments with FabF showed that the H303A (corresponding to H311A in KasA) variant remains active as an acyl-transferase.[49] This result implies that Cys171 in KasA could also be deprotonated regardless of His311. To address this issue, we performed MD simulations for the H311A mutant and compared them with the simulations of the wild-type enzyme in the zwitterionic state. Originally, there are four surrounding residues that form hydrogen bonds with the thiolate ion of Cys171 in wild-type KasA. Those are His345, the backbone amides of Cys171 and Phe404, and His311 via a water molecule. In the MD simulation results for the H311A mutant, the thiolate

dx.doi.org/10.1021/bi200006t |*Biochemistry* 2011, 50, 5743–5756

ion in Cys171 frequently forms temporal interactions with surrounding water molecules. These interactions will also stabilize the negatively charged form, but there was no stable state that lasted for a noticeable time period as in the wild-type protein. The other hydrogen bonds provided by His345 and the backbone amide of Cys171 maintained almost the same distance distributions as in the wild-type protein as shown in Figure 10. However, a remarkable shift to shorter distances was observed in the distance distribution of the hydrogen bond formed between the thiolate and the backbone amide of Phe404. This hydrogen bond stabilizes the thiolate form in the H113A variant considerably more than in the wild-type protein and hence compensates for the missing His311. This strong hydrogen bond was possible because of a conformational change in the side chain of Phe404 as shown in Figure 10.

FEP Calculations for Evaluating the Perturbed pK_a Value of Cys171 in the H311A Mutant. To further analyze the hypothesis mentioned above, we used the FEP method to compute the pK_a shift of Cys171 in the H311A variant. Because the conformational change of the side chain of Phe404 was expected to be critical for shifting the pK_a value of Cys171, one of the frames after this conformational change had taken place was used as a starting structure for the FEP calculations. The corresponding thermodynamic cycle is provided in the bottom part of Figure 6. The results are listed in the second column of Table 2. The resulting pK_a value of Cys171 in the H311A mutant is around 6.7. If Phe404 stays in a position similar to that in the wild-type protein, the corresponding pK_a value is around 8.3. In line with our structural results, this indicates that the mutant can be active because the stabilization of the thiolate is compensated by Phe404.

DISCUSSION

KasA represents an attractive drug target against tuberculosis because its depletion gives rise to cell lysis and cell death. The development of new agents requires detailed information about the structure and function of the active site. Structural data are the methods of choice for this analysis; however, the positions of hydrogen atoms in most cases cannot be determined, and the crystal structure can characterize only the energetically lowest conformer. This study provides additional information by means of MD simulation and FEP and QM/MM computations in combination with the umbrella sampling method. Using this combined methodology, we were able to shed light on the protonation state of the active site of KasA. Furthermore, a picture that indicates how different moieties (water molecules and residues) influence the functionality of the enzyme emerges.

The simulations were initiated from the X-ray data provided by Luckner et al.[47] To obtain information about the protonation status, we performed MD simulations for all possible tautomers and compared the computed structural behavior with the experimental X-ray data. The best agreement was obtained for the protonation status of the zwitterionic state as indicated in Figure 11. The data obtained for the negatively charged state (Figure 5) also do not deviate strongly, but FEP computations reliably showed that the zwitterionic state is lower in energy. In line with the structural data, QM/MM computations in combination with the umbrella sampling method also predict the zwitterionic state to be lower in energy than the neutral state. However, the energy difference seems to be so small that both states should be populated at body temperature. An analysis of the structural changes also indicates that the enzyme can easily switch between both states.

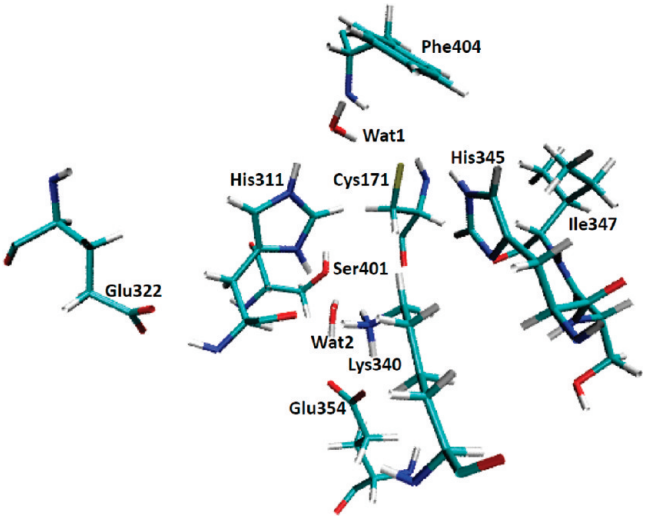

Figure 11. Geometrical orientation of the zwitterionic resting state of KasA predicted in this work.

The MD simulation also allowed insights into the role of the different moieties in the vicinity of the active site. They reliably showed that a hydrogen bonding network including Glu354, Lys340, Ser401, and Wat2 fixes the imidazole ring of His311 in the position needed for the enzymatic reaction. In this network, Wat2 represents the anchor for His311 while the other residues keep the Wat2 molecule in its position. An additional hydrogen bond between Lys340 and the backbone carbonyl group of His311 provides extra stability. However, MD simulations showed without doubt that Wat2 is most important. If it is removed, the orientation of the active site changes in a way that in all probability the enzyme becomes inactive.

Our computational analysis predicts that the zwitterionic state given in Figure 11 represents the resting state of the KasA enzyme. This supports the mechanism for the acyl-transfer step of the Claisen condensation suggested by Olsen et al.[50] The acyl transfer starts with an attack of the negatively charged Cys171 sulfur center that is present in the zwitterionic state but not in the neutral state. Furthermore, the zwitterionic state can catalyze the elimination of the S-AcpM group by providing the proton from the N_ε center of His311 (Scheme 2). This framework makes the overall reaction thermodynamically more favorable because a negatively charged thiolate (Cys171) attacks while a neutral thiol (HS-AcpM) is eliminated. Because of the transfer of the proton to the leaving group, the imidazole ring of His311 can accept the proton from malonyl-ACP. This transfer represents the initial step of the decarboxylation step of the Claisen condensation.

The charge deletion analysis shows that the contribution from the helix macrodipole to stabilize the zwitterionic state was very small in comparison to the effects arising from other residues. This is contrary to the idea that this helix macrodipole is the main reason why the catalytic cysteine residues are often deprotonated. However, a similar case has been reported for cathepsin B.[21] The remarkable contribution of the Glu322 residue to the stabilization of the zwitterionic state is another surprising result because this residue is positioned near the backbone of His311, i.e., far from Cys171 (Figure 11). In the wild-type protein, Glu322 does not directly stabilize the thiolate form of Cys171.

Scheme 2. Illustration of the Mechanism for the Acyl Transfer Involving a Tetrahedral KasA−Fatty Acid−ACP Complex Intermediate

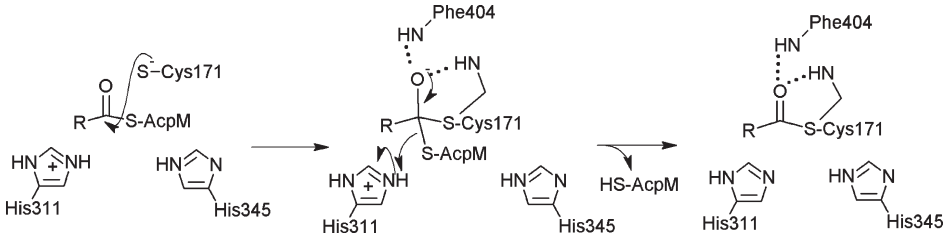

It enhances the basicity of His311 so that an abstraction of the proton from Cys171 by His311 becomes possible. Through its water-mediated hydrogen bond, His311 in turn stabilizes the thiolate moiety of Cys171. In the H311A mutant, this stabilization is no longer possible, but the negatively charged thiolate remains because it is stabilized through its interaction with Phe404. Thus, the acyl transfer remains feasible in H311A.

AUTHOR INFORMATION

Corresponding Author

*Phone: (+49)931 31-85394. Fax: (+49)931-888-5331. E -mail: bernd@chemie.uni-wuerzburg.de.

Funding Sources

Financial support by the DFG (Deutsche Forschungsgemeinschaft) in the framework of SFB 630 and FZ82 is gratefully acknowledged.

ACKNOWLEDGMENT

We thank Prof. H. Schindelin (University of Würzburg) for helpful discussions.

ABBREVIATIONS

KasA, β-ketoacyl ACP synthase I; MD, molecular dynamics; FEP, free energy perturbation; QM/MM, hybrid quantum mechanics and molecular dynamics; TB, tuberculosis; MDR-TB, multidrug-resistant tuberculosis; XDR-TB, extensively drug-resistant tuberculosis; FAS, fatty acid synthesis; AcpM, acyl carrier protein; PDB, Protein Data Bank; HDLC, hybrid delocalized internal coordinate; QM, quantum mechanics; MM, molecular mechanics; PES, potential energy surface; PMF, potential of mean force.

REFERENCES

(1) World Health Organization (2008) Global tuberculosis control: Surveillance, planning, financing. http://www.who.int/tb/publications/global_report/2008/en/index.html.

(2) Jain, A., and Mondal, R. (2008) Extensively drug-resistant tuberculosis: Current challenges and threats. *FEMS Immunol. Med. Microbiol. 53*, 145–150.

(3) Shenoi, S., and Friedland, G. (2009) Extensively Drug-Resistant Tuberculosis: A New Face to an Old Pathogen. *Annu. Rev. Med. 60*, 307–320.

(4) Hong, X., and Hopfinger, A. J. (2004) Molecular Modeling and Simulation of *Mycobacterium tuberculosis* Cell Wall Permeability. *Biomacromolecules 5*, 1066–1077.

(5) Dubnau, E., Chan, J., Raynaud, C., Mohan, V. P., Lanéelle, M., Yu, K., Quémard, A., Smith, I., and Daffé, M. (2000) Oxygenated mycolic acids are necessary for virulence of *Mycobacterium tuberculosis* in mice. *Mol. Microbiol. 36*, 630–637.

(6) Glickman, M. S., Cox, J. S., and Jacobs, W. R. (2000) A Novel Mycolic Acid Cyclopropane Synthetase Is Required for Cording, Persistence, and Virulence of *Mycobacterium tuberculosis*. *Mol. Cell 5*, 717–727.

(7) Glickman, M. S., and Jacobs, W. R. (2001) Microbial Pathogenesis of *Mycobacterium tuberculosis*: Dawn of a Discipline. *Cell 104*, 477–485.

(8) Slayden, R., Lee, R., Armour, J., Cooper, A., Orme, I., Brennan, P., and Besra, G. (1996) Antimycobacterial action of thiolactomycin: An inhibitor of fatty acid and mycolic acid synthesis. *Antimicrob. Agents Chemother. 40*, 2813–2819.

(9) Kremer, L., Douglas, J. D., Baulard, A. R., Morehouse, C., Guy, M. R., Alland, D., Dover, L. G., Lakey, J. H., Jacobs, W. R., Brennan, P. J., Minnikin, D. E., and Besra, G. S. (2000) Thiolactomycin and Related Analogues as Novel Anti-mycobacterial Agents Targeting KasA and KasB Condensing Enzymes in *Mycobacterium tuberculosis*. *J. Biol. Chem. 275*, 16857–16864.

(10) Zhang, H., Machutta, C. A., and Tonge, P. J. (2010) Fatty Acid Biosynthesis and Oxidation. In *Comprehensive Natural Products II*, pp 231−275, Elsevier, Oxford, U.K.

(11) Smith, S., Witkowski, A., and Joshi, A. K. (2003) Structural and functional organization of the animal fatty acid synthase. *Prog. Lipid Res. 42*, 289–317.

(12) Lu, Y.-J., Zhang, Y.-M., and Rock, C. O. (2004) Product diversity and regulation of type II fatty acid synthases. *Biochem. Cell Biol. 82*, 145–155.

(13) Campbell, J. W., and Cronan, J. E. (2001) Bacterial Fatty Acid Biosynthesis: Targets for Antibacterial Drug Discovery. *Annu. Rev. Microbiol. 55*, 305–332.

(14) Kremer, L., Dover, L. G., Carrère, S., Nampoothiri, K. M., Lesjean, S., Brown, A. K., Brennan, P. J., Minnikin, D. E., Locht, C., and Besra, G. S. (2002) Mycolic acid biosynthesis and enzymic characterization of the β-ketoacyl-ACP synthase A-condensing enzyme from *Mycobacterium tuberculosis*. *Biochem. J. 364*, 423–430.

(15) Bhatt, A., Kremer, L., Dai, A. Z., Sacchettini, J. C., and Jacobs, W. R. (2005) Conditional Depletion of KasA, a Key Enzyme of Mycolic Acid Biosynthesis, Leads to Mycobacterial Cell Lysis. *J. Bacteriol. 187*, 7596–7606.

(16) Bhatt, A., Molle, V., Besra, G. S., Jacobs, W. R., Jr., and Kremer, L. (2007) The *Mycobacterium tuberculosis* FAS-II condensing enzymes: Their role in mycolic acid biosynthesis, acid-fastness, pathogenesis and in future drug development. *Mol. Microbiol. 64*, 1442–1454.

(17) White, S. W., Zheng, J., Zhang, Y.-M., and Rock, C. O. (2005) The Structural Biology of Type II Fatty Acid Biosynthesis. *Annu. Rev. Biochem. 74*, 791–831.

(18) Huang, W., Jia, J., Edwards, P., Dehesh, K., Schneider, G., and Lindqvist, Y. (1998) Crystal structure of β-ketoacyl-acyl carrier protein synthase II from *E. coli* reveals the molecular architecture of condensing enzymes. *EMBO J. 17*, 1183–1191.

(19) Moche, M., Dehesh, K., Edwards, P., and Lindqvist, Y. (2001) The crystal structure of β-ketoacyl-acyl carrier protein synthase II from *Synechocystis* sp. at 1.54 Å resolution and its relationship to other condensing enzymes. *J. Mol. Biol. 305*, 491–503.

(20) McGuire, K. A., Siggaard-Andersen, M., Bangera, M. G., Olsen, J. G., and von Wettstein-Knowles, P. (2001) β-Ketoacyl-[Acyl Carrier Protein] Synthase I of *Escherichia coli*: Aspects of the Condensation Mechanism Revealed by Analyses of Mutations in the Active Site Pocket. *Biochemistry 40*, 9836–9845.

(21) Mladenovic, M., Fink, R. F., Thiel, W., Schirmeister, T., and Engels, B. (2008) On the Origin of the Stabilization of the Zwitterionic Resting State of Cysteine Proteases: A Theoretical Study. *J. Am. Chem. Soc. 130*, 8696–8705.

(22) Phillips, J. C., Braun, R., Wang, W., Gumbart, J., Tajkhorshid, E., Villa, E., Chipot, C., Skeel, R. D., Kalé, L., and Schulten, K. (2005) Scalable molecular dynamics with NAMD. *J. Comput. Chem. 26*, 1781–1802.

(23) MacKerell, A. D., Jr., Bashford, D., Bellott, M., Dunbrack, R. L., Jr., Evanseck, J. D., Field, M. J., Fischer, S., Gao, J., Guo, H., Ha, S., Joseph-McCarthy, D., Kuchnir, L., Kuczera, K., Lau, F. T. K., Mattos, C., Michnick, S., Ngo, T., Nguyen, D. T., Prodhom, B., Reiher, W. E., Roux, B., Schlenkrich, M., Smith, J. C., Stote, R., Straub, J., Watanabe, M., Wiórkiewicz-Kuczera, J., Yin, D., and Karplus, M. (1998) All-Atom Empirical Potential for Molecular Modeling and Dynamics Studies of Proteins. *J. Phys. Chem. B 102*, 3586–3616.

(24) Mackerell, A. D., Jr., Feig, M., and Brooks, C. L., III (2004) Extending the treatment of backbone energetics in protein force fields: Limitations of gas-phase quantum mechanics in reproducing protein conformational distributions in molecular dynamics simulations. *J. Comput. Chem. 25*, 1400–1415.

(25) Foloppe, N., Sagemark, J., Nordstrand, K., Berndt, K. D., and Nilsson, L. (2001) Structure, dynamics and electrostatics of the active site of glutaredoxin 3 from *Escherichia coli*: Comparison with functionally related proteins. *J. Mol. Biol. 310*, 449–470.

(26) Jorgensen, W. L., Chandrasekhar, J., Madura, J. D., Impey, R. W., and Klein, M. L. (1983) Comparison of simple potential functions for simulating liquid water. *J. Chem. Phys. 79*, 926.

(27) Hestenes, M., and Stiefel, E. (1952) Methods of Conjugate Gradients for Solving Linear Systems. *J. Res. Natl. Inst. Stand. Technol. 49*, 409–436.

(28) Andersen, H. C. (1983) Rattle: A "velocity" version of the shake algorithm for molecular dynamics calculations. *J. Comput. Phys. 52*, 24–34.

(29) Zwanzig, R. W. (1955) High-Temperature Equation of State by a Perturbation Method. II. Polar Gases. *J. Chem. Phys. 23*, 1915.

(30) Pitera, J. W., and van Gunsteren, W. F. (2002) A Comparison of Non-Bonded Scaling Approaches for Free Energy Calculations. *Mol. Simul. 28*, 45.

(31) Lu, N., and Kofke, D. A. (2001) Accuracy of free-energy perturbation calculations in molecular simulation. I. Modeling. *J. Chem. Phys. 114*, 7303.

(32) Sherwood, P., de Vries, A. H., Guest, M. F., Schreckenbach, G., Catlow, C. R. A., French, S. A., Sokol, A. A., Bromley, S. T., Thiel, W., Turner, A. J., Billeter, S., Terstegen, F., Thiel, S., Kendrick, J., Rogers, S. C., Casci, J., Watson, M., King, F., Karlsen, E., Sjøvoll, M., Fahmi, A., Schäfer, A., and Lennartz, C. (2003) QUASI: A general purpose implementation of the QM/MM approach and its application to problems in catalysis. *THEOCHEM 632*, 1–28.

(33) *TURBOMOLE*, version 6.1 (2009) University of Karlsruhe and Forschungszentrum Karlsruhe GmbH, from 1989 to 2007, TURBOMOLE GmbH, since 2007 (http://www.turbomole.com).

(34) Smith, W., and Forester, T. R. (1996) DL_POLY_2.0: A general-purpose parallel molecular dynamics simulation package. *J. Mol. Graphics 14*, 136–141.

(35) Sherwood, P., de Vries, A. H., Collins, S. J., Greatbanks, S. P., Burton, N. A., Vincent, M. A., and Hillier, I. H. (1997) Computer simulation of zeolite structure and reactivity using embedded cluster methods. *Faraday Discuss. 106*, 79–92.

(36) Klamt, A., and Schuerrmann, G. (1993) COSMO: A new approach to dielectric screening in solvents with explicit expressions for the screening energy and its gradient. *J. Chem. Soc., Perkin Trans. 2*, 799.

(37) Billeter, S. R., Turner, A. J., and Thiel, W. (2000) Linear scaling geometry optimization and transition state search in hybrid delocalised internal coordinates. *Phys. Chem. Chem. Phys. 2*, 2177–2186.

(38) Rocha, G. B., Freire, R. O., Simas, A. M., and Stewart, J. J. P. (2006) RM1: A reparameterization of AM1 for H, C, N, O, P, S, F, Cl, Br, and I. *J. Comput. Chem. 27*, 1101–1111.

(39) Hornak, V., Abel, R., Okur, A., Strockbine, B., Roitberg, A., and Simmerling, C. (2006) Comparison of multiple Amber force fields and development of improved protein backbone parameters. *Proteins 65*, 712–725.

(40) Grossfield, A. *WHAM: The weighted histogram analysis method*, version 2.0.4. http://membrane.urmc.rochester.edu/content/wham.

(41) Case, D., Darden, T., Cheatham, T., Simmerling, C., Wang, J., Duke, R., Luo, R., Crowley, M., Walker, R., Zhang, W., Merz, K., Wang, B., Hayik, S., Roitberg, A., Seabra, G., Kolossváry, I., Wong, K., Paesani, F., Vanicek, J., Wu, X., Brozell, S., Steinbrecher, T., Gohlke, H., Yang, L., Tan, C., Mongan, J., Hornak, V., Cui, G., Mathews, D., Seetin, M., Sagui, C., Babin, V., and Kollman, P. (2010) *Amber 11*, University of California, San Francisco.

(42) Walker, R. C., Crowley, M. F., and Case, D. A. (2008) The implementation of a fast and accurate QM/MM potential method in Amber. *J. Comput. Chem. 29*, 1019–1031.

(43) Bash, P. A., Field, M. J., Davenport, R. C., Petsko, G. A., Ringe, D., and Karplus, M. (1991) Computer simulation and analysis of the reaction pathway of triosephosphate isomerase. *Biochemistry 30*, 5826–5832.

(44) Mulholland, A. J., and Richards, W. G. (1997) Acetyl-CoA enolization in citrate synthase: A quantum mechanical/molecular mechanical (QM/MM) study. *Proteins 27*, 9–25.

(45) Wong, K. F., Watney, J. B., and Hammes-Schiffer, S. (2004) Analysis of Electrostatics and Correlated Motions for Hydride Transfer in Dihydrofolate Reductase. *J. Phys. Chem. B 108*, 12231–12241.

(46) von Wettstein-Knowles, P., Olsen, J. G., McGuire, K. A., and Henriksen, A. (2006) Fatty acid synthesis. Role of active site histidines and lysine in Cys-His-His-type β-ketoacyl-acyl carrier protein synthases. *FEBS J. 273*, 695–710.

(47) Luckner, S. R., Machutta, C. A., Tonge, P. J., and Kisker, C. (2009) Crystal Structures of *Mycobacterium tuberculosis* KasA Show Mode of Action within Cell Wall Biosynthesis and its Inhibition by Thiolactomycin. *Structure 17*, 1004–1013.

(48) Price, A. C., Rock, C. O., and White, S. W. (2003) The 1.3-Angstrom-resolution crystal structure of β-ketoacyl-acyl carrier protein synthase II from *Streptococcus pneumoniae*. *J. Bacteriol. 185*, 4136–4143.

(49) Zhang, Y.-M., Hurlbert, J., White, S. W., and Rock, C. O. (2006) Roles of the active site water, histidine 303, and phenylalanine 396 in the catalytic mechanism of the elongation condensing enzyme of *Streptococcus pneumoniae*. *J. Biol. Chem. 281*, 17390–17399.

(50) Olsen, J. G., Kadziola, A., von Wettstein-Knowles, P., Siggaard-Andersen, M., and Larsen, S. (2001) Structures of β-ketoacyl-acyl carrier protein synthase I complexed with fatty acids elucidate its catalytic machinery. *Structure 9*, 233–243.